UNCLASSIFIED DTIC FILE COPY MASTER COPY - FOR REPRODUCTION PURPOSES

SECURITY CLASSIFICATION OF THIS PAGE

(2)

ORT DOCUMENTATION PAGE

1a. **AD-A201 378**

1b. RESTRICTIVE MARKINGS

2a.

2b. ...DOWNGRADING SCHEDULE

3. DISTRIBUTION / AVAILABILITY OF REPORT
Approved for public release; distribution unlimited.

4. PERFORMING ORGANIZATION REPORT NUMBER(S)

5. MONITORING ORGANIZATION REPORT NUMBER(S)
ARO 22349.19-CH

6a. NAME OF PERFORMING ORGANIZATION
The Johns Hopkins University

6b. OFFICE SYMBOL (If applicable)

7a. NAME OF MONITORING ORGANIZATION
U. S. Army Research Office

6c. ADDRESS (City, State, and ZIP Code)
Department of Chemistry
34th and Charles Sts.
Baltimore, MD 21218

7b. ADDRESS (City, State, and ZIP Code)
P. O. Box 12211
Research Triangle Park, NC 27709-2211

8a. NAME OF FUNDING / SPONSORING ORGANIZATION
U. S. Army Research Office

8b. OFFICE SYMBOL (If applicable)

9. PROCUREMENT INSTRUMENT IDENTIFICATION NUMBER
DAAG29-85-K-0018

8c. ADDRESS (City, State, and ZIP Code)
P. O. Box 12211
Research Triangle Park, NC 27709-2211

10. SOURCE OF FUNDING NUMBERS

PROGRAM ELEMENT NO.	PROJECT NO.	TASK NO.	WORK UNIT ACCESSION NO.

11. TITLE (Include Security Classification)
Collisional Transfer between and Quenching of the $3p\ ^3P$ and ^5P States of the Oxygen Atom

12. PERSONAL AUTHOR(S)
Paul J. Dagdigian, Brad F. Forch, and Andrzej W. Miziolek

13a. TYPE OF REPORT	13b. TIME COVERED FROM ____ TO ____	14. DATE OF REPORT (Year, Month, Day)	15. PAGE COUNT
Reprint			

16. SUPPLEMENTARY NOTATION
The view, opinions and/or findings contained in this report are those of the author(s) and should not be construed as an official Department of the Army position, policy, or decision, unless so designated by other documentation.

17. COSATI CODES		
FIELD	GROUP	SUB-GROUP

18. SUBJECT TERMS (Continue on reverse if necessary and identify by block number)
Electronic quenching, excitation transfer, oxygen atom.

19. ABSTRACT (Continue on reverse if necessary and identify by block number)

ABSTRACT ON REPRINT

DTIC ELECTED OCT 2 0 1988 D

20. DISTRIBUTION / AVAILABILITY OF ABSTRACT
☐ UNCLASSIFIED/UNLIMITED ☐ SAME AS RPT. ☐ DTIC USERS

21. ABSTRACT SECURITY CLASSIFICATION
Unclassified

22a. NAME OF RESPONSIBLE INDIVIDUAL

22b. TELEPHONE (Include Area Code)

22c. OFFICE SYMBOL

DD FORM 1473, 84 MAR 83 APR edition may be used until exhausted. All other editions are obsolete.

SECURITY CLASSIFICATION OF THIS PAGE
UNCLASSIFIED

Collisional quenching and excitation transfer between the oxygen atom 3p ^3P and ^5P states have been investigated in a discharge flow apparatus with O_2 and N_2 collisional partners. The ^3P state was excited by two-photon excitation at 225.6 nm from the $2p^4\ ^3P$ ground state, and temporal profiles of the $^3P \rightarrow {}^3S$ and $^5P \rightarrow {}^5S$ emission at 844.7 and 777.5 nm, respectively, to the lower 3s manifold were recorded. From an analysis of ^3P decay curves as a function of quencher pressure, bimolecular rate constants for the removal of the ^3P state were determined: $k_3^Q(O_2) = (7.8 \pm 0.8) \times 10^{-10}$ and $k_3^Q(N_2) = (5.87 \pm 0.15) \times 10^{-10}$ molecule^{-1} cm^3 s^{-1}. The intercept of the O_2 Stern-Volmer plot yielded $k_3^r = 2.98 \pm 0.15) \times 10^7$ s^{-1} for the ^3P radiative decay rate. The collisional quenching rate constant for the ^5P state by O_2 was obtained by analysis of ^5P decay curves: $k_5^Q(O_2) = (10.8 \pm 1.8) \times 10^{-10}$ molecule^{-1} cm^3 s^{-1}. Rate constants k_{35} for $^3P \rightarrow {}^5P$ excitation transfer were obtained from the ratio of the $^5P \rightarrow {}^5S$ to $^3P \rightarrow {}^3S$ emission intensities as a function of quencher pressure: $k_{35}(O_2) \approx 6 \times 10^{-11}$ and $k_{35}(N_2) \approx 2 \times 10^{-11}$ molecule^{-1} cm^3 s^{-1}.

COLLISIONAL TRANSFER BETWEEN AND QUENCHING OF THE 3p ^{3}P AND ^{5}P STATES OF THE OXYGEN ATOM

Paul J. DAGDIGIAN
Department of Chemistry, The Johns Hopkins University, Baltimore, MD 21218, USA

Brad E. FORCH and Andrzej W. MIZIOLEK
US Army Ballistic Research Laboratory, Aberdeen Proving Ground, MD 21005-5066, USA

Received 4 March 1988; in final form 4 May 1988

Collisional quenching and excitation transfer between the oxygen atom 3p ^{3}P and ^{5}P states have been investigated in a discharge flow apparatus with O_2 and N_2 collisional partners. The ^{3}P state was excited by two-photon excitation at 225.6 nm from the $2p^4\,^3P$ ground state, and temporal profiles of the $^3P \rightarrow {}^3S$ and $^5P \rightarrow {}^5S$ emission at 844.7 and 777.5 nm, respectively, to the lower 3s manifold were recorded. From an analysis of ^{3}P decay curves as a function of quencher pressure, bimolecular rate constants for the removal of the ^{3}P state were determined: $k_3^Q(O_2) = (7.8 \pm 0.8) \times 10^{-10}$ and $k_3^Q(N_2) = (5.87 \pm 0.15) \times 10^{-10}$ molecule^{-1} cm^3 s^{-1}. The intercept of the O_2 Stern–Volmer plot yielded $k_3^r = (2.98 \pm 0.15) \times 10^7$ s^{-1} for the ^{3}P radiative decay rate. The collisional quenching rate constant for the ^{5}P state by O_2 was obtained by analysis of ^{5}P decay curves: $k_5^Q(O_2) = (10.8 \pm 1.8) \times 10^{-10}$ molecule^{-1} cm^3 s^{-1}. Rate constants k_{35} for $^3P \rightarrow {}^5P$ excitation transfer were obtained from the ratio of the $^5P \rightarrow {}^5S$ to $^3P \rightarrow {}^3S$ emission intensities as a function of quencher pressure: $k_{35}(O_2) \approx 6 \times 10^{-11}$ and $k_{35}(N_2) \approx 2 \times 10^{-11}$ molecule^{-1} cm^3 s^{-1}.

1. Introduction

There is a considerable need for well-characterized diagnostic techniques for the quantitative measurement of the concentrations of species in flames and other combustion environments. The use of multiphoton excitation schemes for the detection of light atoms, such as oxygen, has drawn considerable interest in recent years [1–13]. Two different approaches have been employed in these methods, namely observation of the fluorescence emission from the multiphoton-excited resonant state [1–9] or absorption of an additional photon to produce ionization [9–13]. Both of these schemes have been utilized for the detection of hydrogen and oxygen atoms in flames. The former method has advantages over the latter in that it does not require the insertion of a probe into the medium and can also be used to obtain two-dimensional images of atomic concentrations in flames, as has recently been demonstrated [14,15]. It is also easier to discriminate against background photon emission than ionization.

Fig. 1 illustrates the scheme which has been used for the detection of oxygen atoms [1,3,5–7,9,14,15]. Here, oxygen atoms are excited in a two-photon transition to the 3p ^{3}P state with 225.6 nm laser radiation and are detected by observation of the fluorescent emission to the 3s ^{3}S state at 844.7 nm. A number of parameters are required for the use of this diagnostic tool in a quantitative fashion. Recently, Bamford et al. [9] have reported absolute cross sections for the two-photon absorption process, as well as for one-photon photoionization of the ^{3}P state. Bimolecular collision quenching rate constants for this state have also been measured by several groups [1,6,7,9]. These data are required to account for collisional effects in finite-pressure environments.

Miziolek and DeWilde [5] have also shown the potential importance of collisional excitation transfer processes in the collisional removal of this highly excited atomic state. They excited oxygen atoms by two-photon absorption at 225.6 nm in an atmosphere-pressure CH_4–N_2O–N_2 flame and observed within and through the flame front not only $^3P \rightarrow {}^3S$ emission at 844.7 nm, but also $^5P \rightarrow {}^5S$ emission of even greater intensity at 777.5 nm. Similar detection

0 009-2614/88/$ 03.50
(North-Holland Physics Publishing Division)

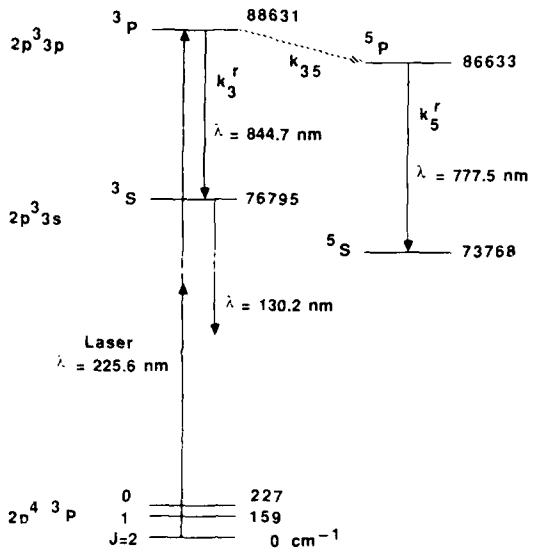

Fig. 1. Relevant energy levels for two-photon excitation of oxygen atoms and excited-state collisional energy transfer. The electronic energies, taken from ref. [16], are given in cm^{-1}, and allowed radiative transitions are denoted, with wavelengths given in nm. The denoted radiative and collisional rate constants are defined in section 3.2.

of 777.5 nm emission was subsequently observed in imaging studies of atomic oxygen in flames [14,15]. These observations suggest the occurrence of excitation transfer from the ^3P to the ^5P state (see fig. 1). The interpretation of these experiments in terms of specific bimolecular rate processes is not straightforward because of the high pressure and chemical complexity of these flames. In addition, at least in the experiment of Miziolek and DeWilde [5], the tightly focused laser probe was observed to be promoting multiphoton photolysis of the oxidizer as well as the fuel molecules, leading to a two-photon resonant formation of a microplasma. Nevertheless, even under conditions of no apparent laser probe volume perturbation, it appears that spin-changing collisions of the initially excited level could be a significant collisional removal pathway for laser-excited oxygen 3p ^3P atoms. In order to employ two-photon excitation for quantitative measurements in combustion environments, such as propellant flames, it is necessary to understand the mechanism for transfer of the initial excitation energy.

The present experimental study was undertaken to investigate collisional excitation transfer from the oxygen 3p ^3P to ^5P states in a controlled low-pressure environment. Previous studies [1,6,7,9] of collisional processes involving the ^3P state have centered on the measurement of total quenching rate constants with closed-shell collisional partners, such as the inert gases, nitrogen molecules, etc. Simple theoretical considerations [17] suggest that open-shell free radical species will be more effective in inducing spin-changing excitation transfer to the ^5P state. Approach of an open-shell perturber species in a state of, say, doublet spin multiplicity to an oxygen atom in the 3p ^3P state will yield both doublet and quartet molecular curves, while approach to the ^5P state yields quartet and sextet states. Crossing of quartet curves originating from the ^3P and ^5P asymptotes will provide a spin-allowed mechanism for collision-induced transitions between the ^3P and ^5P states, which is not possible with closed-shell partners. This argument ignores the possible importance of excitations in the collision partner.

In the present study, we compare the propensity of the stable open-shell oxygen molecule and the closed-shell nitrogen molecule to induce $^3P \rightarrow {}^5P$ transitions. Previous experiments [1,6,7,9] have determined the total bimolecular quenching rate constants for quenching of the ^3P state by these molecules.

2. Experimental

The apparatus employed for these experiments is shown in fig. 2. Oxygen atoms were generated by passing a mixture of helium and oxygen (typical partial pressures of 1.2 and 0.2 Torr, respectively) through an Evenson–Broida 2450 MHz resonant cavity. UHP grade gases were obtained from Linde and used without further purification. The walls of discharge tube were coated with phosphoric acid to reduce atomic recombination on the surfaces [18]. The forward microwave power was kept relatively low (<25 W) in order to minimize the fractional dissociation of the oxygen molecules and production of other transient species. Nevertheless, this production scheme prepared sufficient densities of ground-state oxygen atoms for these experiments. The quenching gases, either N_2 or additional O_2, were

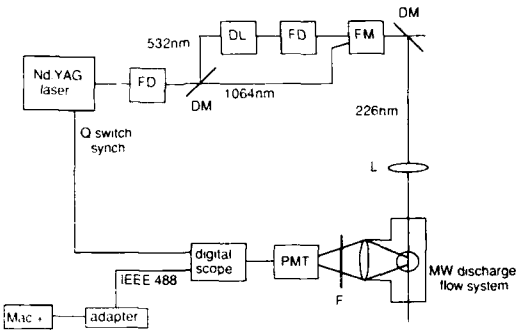

Fig. 2. Schematic diagram of the experimental apparatus. DL: dye laser; FD: frequency-doubling crystal; FM: frequency-mixing crystal; DM: dicroic mirror; L: lens; F: interference filter; PMT: photomultiplier tube.

added downstream of the microwave discharge. Pressures were measured by a capacitance manometer. The flow tube was pumped by a 50 cfm single-stage mechanical pump.

The laser excitation and fluorescence detection zone was located 10 cm beyond a 90° bend Wood's horn light trap, which itself was placed just past the microwave discharge. Two-photon excitation of oxygen atoms was accomplished with tunable UV radiation from a Nd : YAG-pumped, frequency-doubled and mixed dye laser (Quantel) which operated at a 10 Hz repetition rate. The dye solution in the latter was a concentration- and composition-tuned mixture of rhodamine 590 and 610. The 266 nm radiation was separated from other wavelengths by a dichroic mirror: this separation technique was preferred over the use of prisms since, with the former, the laser beam position through the flow system does not change with wavelength. Typical UV power at the apparatus was approximately 1 mJ per pulse, and the bandwidth of the doubled and mixed radiation was $\approx 1\ \mathrm{cm}^{-1}$ fwhm. The radiation was focused into the center of a flow system with a 30 cm Suprasil lens. No photolytic effects due to laser decomposition of molecular oxygen were evident, as observation of the O atom two-photon signal required the presence of both molecular oxygen and microwave radiation.

The fluorescence was collected at right angles to the laser beam with a fast ($f/2$) Suprasil lens and focused through a filter onto a red-sensitive photomultiplier tube (EMI 9516QB). The filters employed were a 850 nm center wavelength, 25 nm bandpass interference filter for detection of the $^3P \rightarrow {}^3S$ emission at 844.7 nm and a 780 nm center wavelength, 10 nm bandpass filter for observation of the $^5P \rightarrow {}^5S$ at 777.5 nm. The measured transmission of these filters was 56 and 66% at 844.7 and 777.5 nm, respectively.

The output from the photomultiplier was passed to a boxcar integrator (Stanford Research Systems) for measuring excitation spectra or to a digital oscilloscope (Tektronix 2430A) for capturing the temporal profiles of fluorescence waveforms. The boxcar integrator and oscilloscope were triggered with a synchronization pulse from the Nd : YAG laser Q switch. Some details about the specifications of the oscilloscope are relevant. The bandwidth of the analog section of this instrument is 125 MHz; the digital sampling rate is 100 megasamples s^{-1}, or 10 ns between channels. In our experiments we utilized an interpolation feature for repetitive signals, which allowed digitization on a finer grid to achieve the full bandwidth: The waveform from an individual laser pulse was obtained with the usual 10 ns spacing; however, successive waveforms were taken with a slightly shifted initial delay, controlled internally by the oscilloscope. To improve the signal-to-noise ratio, waveforms were also acquired using a 256-scan running average. Typical emission lifetimes ranged from 40 to 15 ns, while the laser excitation pulse length was 7 ns.

The waveforms acquired by the digital oscilloscope were transferred through an IEEE 488 interface to a microcomputer (Apple Macintosh Plus) for storage, generation of hard-copy plots, and analysis.

3. Results

3.1. Fluorescence waveforms

Fig. 3 displays typical fluorescence waveforms for emission at 844.7 and 777.5 nm. The noise in these traces is due to the effect of the interpolating feature of the oscilloscope (see section 2) and the large fluctuations in the fluorescence signal between successive laser shots. Under all pressure conditions investigated, the emission at 844.7 nm from the initially excited ^3P level was much stronger. It should

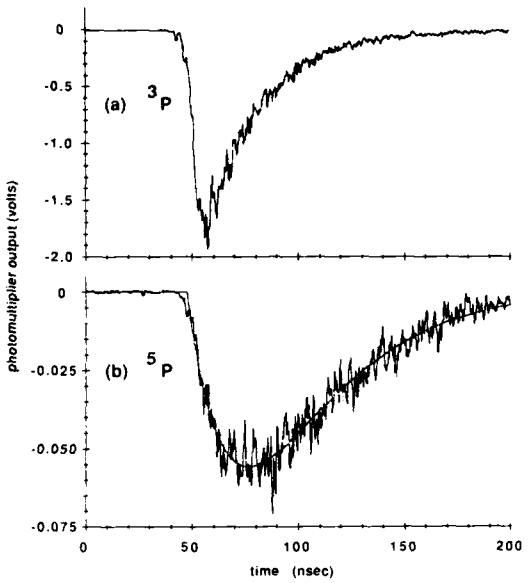

Fig. 3. Waveforms for (a) the $^3P \rightarrow {}^3S$ and (b) the $^5P \rightarrow {}^5S$ fluorescence emission upon two-photon excitation of the 3p ^{3}P state. Pressures: 1.47 Torr He and 0.30 Torr O_2. These waveforms were acquired with the same photomultiplier voltage merely by chaning the detection filter.

also be noted that the relative detection sensitivity (filter transmission plus photomultiplier sensitivity, the latter taken from manufacturer's specifications) was larger (4:1) for the collision-induced $^5P \rightarrow {}^5S$ feature.

In addition to the differing intensities for the fluorescent decay of the initially excited ^{3}P and collisionally populated ^{5}P states, the two waveforms in fig. 3 have different temporal profiles. The waveform for the ^{3}P state in fig. 3a is the usual exponential curve expected for the decay of an excited level, while that for the ^{5}P state in fig. 3b builds up to the peak intensity after an induction period. Section 3.2 presents in detail the equations governing the time dependence of these emissions and shows how rate constants for the various kinetic processes can be extracted.

3.2. Kinetic equations

The following equations govern the kinetics of decay and energy transfer of the 3p ^{3}P and ^{5}P electronic states of the oxygen atom:

$$dn_3/dt = -n_3 k_3 \quad (1)$$

and

$$dn_5/dt = n_3 k_{35} - n_5 k_5, \quad (2)$$

where n_3 and n_5 are the concentrations of the ^{3}P and ^{5}P states, respectively, and k_3 and k_5 are the total removal rates by both radiative and collisional processes for the respective atomic states:

$$k_3 = k_3^r + k_3^Q(\mathrm{M})\ [\mathrm{M}] \quad (3)$$

and

$$k_5 = k_5^r + k_5^Q(\mathrm{M})\ [\mathrm{M}]. \quad (4)$$

Here the spontaneous decay rates are denoted by k_3^r and k_5^r, while the bimolecular quenching rate constants are indicated as $k_3^Q(\mathrm{M})$ and $k_5^Q(\mathrm{M})$. Eqs. (3) and (4) are written assuming there is only one quenching species, of concentration [M], present. The generalization to several collision partners is obvious. These quenching rate constants represent the total rate of collisional removal of the relevant atomic species. The quantity k_{35} in eq. (2) represents that portion of the collisional removal of the ^{3}P state which results in energy transfer to the ^{5}P state:

$$\mathrm{O}(^3\mathrm{P}) + \mathrm{M} \rightarrow \mathrm{O}(^5\mathrm{P}) + \mathrm{M}. \quad (5)$$

We write

$$k_{35} = k_{35}(\mathrm{M})\ [\mathrm{M}], \quad (6)$$

where $k_{35}(\mathrm{M})$ is the bimolecular rate constant for process (5).

We assume that the two-photon laser excitation to the ^{3}P state yields a concentration $n_3^{(0)}$ in this state at $t=0$. Eqs. (1) and (2) may be readily integrated. The ^{3}P state follows a simple exponential decay,

$$n_3 = n_3^{(0)} \exp(-k_3 t), \quad (7)$$

while the time dependence of the ^{5}P state is given by the difference of two exponentials,

$$n_5 = \frac{n_3^{(0)} k_{35} [\exp(-k_5 t) - \exp(-k_3 t)]}{k_3 - k_5}. \quad (8)$$

Thus, we see that the time dependence of the ^{3}P population follows the usual exponential decay, while that of the ^{5}P state builds up to a maximum after some delay.

Eq. (7) shows that the ^{3}P radiative lifetime and

quenching rate constants may be determined by measurement of the decay lifetime $\tau = k_3^{-1}$ as a function of quench gas pressure, in the usual Stern–Volmer treatment. The corresponding quantities for the ^5P state must be determined in a non-linear least-squares treatment of the ^5P concentration as a function of time, according to eq. (8). The time dependence of the ^3P and ^5P concentrations can be determined from the emission intensities at 844.7 and 777.5 nm, respectively.

The $^3P \rightarrow {}^5P$ transfer rate k_{35} cannot be determined from analysis of the fluorescence waveforms alone, but rather from the ratio of the integrated emission intensities. The integrated fluorescence intensity for the decay of the ^3P state is proportional to

$$I_3 = k_3^r \int_0^\infty n_3 \, dt. \tag{9a}$$

With the help of eq. (7), this equals

$$I_3 = n_3^{(0)} (k_3^r / k_3). \tag{9b}$$

The quantity in parentheses in eq. (9b) may be identified with the fluorescence quantum yield for the ^3P state. The integrated emission intensity for the ^5P state is given by

$$I_5 = k_5^r \int_0^\infty n_5 \, dt, \tag{10a}$$

which, with eq. (8), becomes

$$I_5 = k_{35} n_3^{(0)} k_5^r / k_5 k_3. \tag{10b}$$

Thus, the ratio of these integrated emission intensities equals

$$I_5 / I_3 = (k_{35} / k_3^r) \, (k_5^r / k_5). \tag{11}$$

The rightmost quantity in parentheses in eq. (11) is the ^5P fluorescence quantum yield, while the ratio of k_{35}/k_3^r represents the ratio of $^3P \rightarrow {}^5P$ energy transfer collisions to ^3P radiative decay events.

3.3. Quenching rate constants

Quenching rate constants for the ^3P state were determined from linear least-squares fits of the logarithm of the $^3P \rightarrow {}^3S$ emission as a function of time from fluorescence decay curves, similar to that presented in fig. 3a, at different quencher concentrations. A Stern–Volmer plot for O_2 is presented in fig. 4a. In this figure, the abscissa is the total O_2 partial pressure including oxygen passing through the microwave discharge and added downstream. For measurement of both O_2 and N_2 quenching rate constants, helium and oxygen, at typical pressures of approximately 1.3 and 0.2 Torr, respectively, were passed through the discharge. Using the previously measured [6,7] quenching rate constant for helium, we calculate that collisional removal by this species is small under our conditions, approximately 0.07×10^7 s^{-1}. In principle, the transient free radical species generated by the discharge could also contribute to collisional quenching. However, we found that the decay rate k_3 was the same with low (20 W) or high (50 W) microwave power applied to the cavity.

Linear least-squares fits (the solid line in fig. 4a) of these data yields the following bimolecular rate

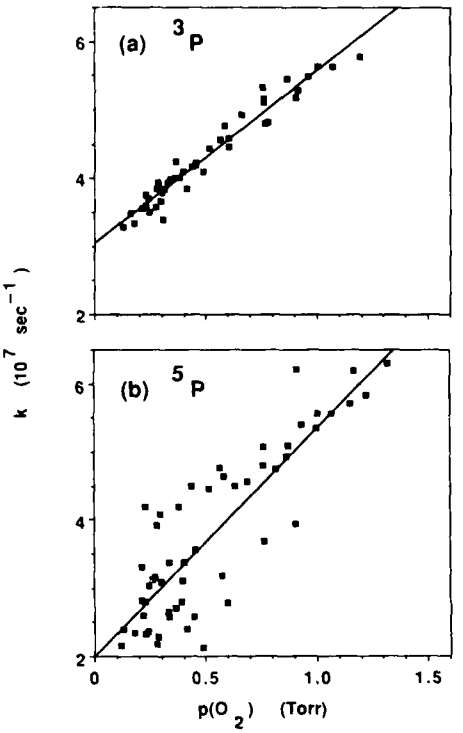

Fig. 4. Stern–Volmer plots for (a) the $^3P \rightarrow {}^3S$ emission at 844.7 nm and (b) the $^5P \rightarrow {}^5S$ emission at 777.5 nm as a function of O_2 quencher partial pressure.

constants listed in table 1 for the total collisional removal rate of the ^3P state. The intercept for the O_2 plot yields a decay rate of $(3.05\pm0.15)\times10^7$ s^{-1}. Correcting for the expected contribution due to helium quenching (see above), we obtain the radiative decay rate for the ^3P state: $k_3^r=(2.98\pm0.15)\times10^7$ s^{-1}. This corresponds to an estimated ^3P radiative lifetime of 33.3 ± 1.7 ns. The quoted uncertainties for all rate constants represent three standard deviations.

The collisional and radiative decay rate for the ^5P state was obtained from analysis of $^5P\rightarrow{}^5S$ decay curves such as that presented in fig. 3b. Because of the weakness of the $^5P\rightarrow{}^5S$ emission signals, this analysis was carried out only for O_2 quencher. The total decay rate k_5 was determined by non-linear least-squares fits [19] using the expected functional form in eq. (8) for the time dependence of the ^5P population. In this fit, the decay rate k_3 for the ^3P state was fixed at the value calculated from the Stern–Volmer plot in fig. 4a for the O_2 partial pressure in the given scan. Parameters allowed to vary in this non-linear fit were the decay rate k_5, an overall normalization constant (proportional to k_{35}), and the channel for which $t=0$. The solid line in fig. 3b represents the fit to the experimental data given in that plot.

The derived decay rates k_5 from non-linear least-squares analysis of $^5P\rightarrow{}^5S$ emission waveforms are presented in fig. 4b. It can be seen that the scatter of the calculated rate constants is large. This is due mainly to the smallness of these emission signals, which arise not directly from the initially populated state but rather by collisional transfer. A Stern–Volmer analysis of these rate constants was performed (solid line in fig. 4b) and yield the following estimates for the bimolecular quenching rate constant by O_2 and the radiative decay rate: $k_5^Q(O_2)=(10.8\pm1.8)\times10^{-10}$ molecule^{-1} cm^3 s^{-1} (included in table 1) and $k_5^r=(2.01\pm0.35)\times10^7$ s^{-1}. This corresponds to an estimated radiative lifetime of 50 ± 9 ns.

3.4. Energy transfer rate constants

Eq. (11) shows that measurement of the ratio of the integrated emission intensities for $^5P\rightarrow{}^5S$ and $^3P\rightarrow{}^3S$ fluorescence decay can yield the rate constant k_{35} for collisional transfer from the ^3P to the ^5P state. Accordingly, a series of experiments were carried out to record these waveforms under identical pressure conditions. For a given partial pressure of added quench gas, the fluorescence waveform for one of these radiative decay paths was recorded; then the filter was switched and the other recorded immediately thereafter. The integrated signals were calculated and their ratios corrected for the relative detection sensitivity at 844.7 and 777.5 nm.

Fig. 5 displays the derived integrated $^5P\rightarrow{}^5S$ to $^3P\rightarrow{}^3S$ intensity ratios, corrected for the wavelength response of the photomultiplier, as a function of both added O_2 and added N_2 gas. The scatter in these data is again large, reflecting the large fluctuations in the fluorescence signal from laser shot to shot. Nevertheless, it can be seen that for both collision partners this ratio is always small and never increases beyond 5%.

In spite of the large experimental uncertainties in

Table 1
Bimolecular rate constants for quenching and collisional transfer of the 3p ^3P and ^5P states of the oxygen atom at room temperature

Collision partner	Rate constant (molecule^{-1} cm^3 s^{-1})	This study	Previous determinations
O_2	k_3^Q	$(7.8\pm0.8)\times10^{-10}$	$(8.64\pm0.16)\times10^{-10}$ [9]
			$(6.3\pm0.12)\times10^{-10}$ [7]
	k_5^Q	$(10.8\pm1.8)\times10^{-10}$	
	k_{35}	6×10^{-11} [a]	
N_2	k_3^Q	$(5.87\pm0.15)\times10^{-10}$	$(4.3\pm0.74)\times10^{-10}$ [7]
			$(2.5\pm0.1)\times10^{-10}$ [1]
	k_{35}	2×10^{-11} [a]	

[a] Estimated experimental uncertainty of a factor of 2.

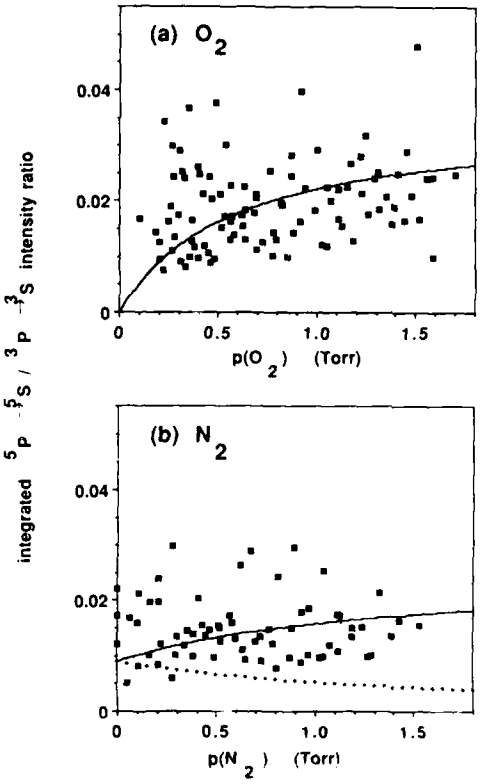

Fig. 5. Ratio of the integrated $^5P \rightarrow {}^5S$ to $^3P \rightarrow {}^3S$ emission intensity (corrected for the wavelength sensitivity of the photomultiplier) versus added (a) O_2 and (b) N_2. The solid curves represent the best fits to the intensity ratio versus quench gas pressure. The dotted curve in (b) shows the expected intensity ratio if $k_{35}(N_2)$ were equal to zero.

the integrated intensity ratio, we may still obtain estimates of the rate constants for $^3P \rightarrow {}^5P$ collisional transfer. For the case of O_2, for which the data are displayed in fig. 5a, the integrated intensity ratio can be expressed as a function of the O_2 density $n(O_2)$ as

$$\frac{I_5}{I_3} = \frac{An(O_2)}{1+n(O_2)/n_O}, \tag{12}$$

where

$$A = k_{35}(O_2)/k_3^r \tag{13}$$

and

$$n_O = k_5^r/k_5^Q(O_2). \tag{14}$$

The quantity n_O can be calculated from the Stern–Volmer analysis (fig. 4b) for the ^5P state and equals 1.9×10^{16} molecules cm^{-3} (or 0.58 Torr).

Thus, eq. (12) can be fit to the data in fig. 5a by a linear least-squares fit [19] to determine the coefficient A in eq. (12). Using our derived value for the ^3P radiative decay rate k_3^r, we find that the rate constant $k_{35}(O_2)$ equals 6×10^{-11} molecule^{-1} cm^3 s^{-1}. We estimate an uncertainty of approximately a factor of 2 in this value, due to the scatter in the determined intensity ratios given in fig. 5 and the uncertainty in the relative detection sensitivity. The contribution to the uncertainty in $k_{35}(O_2)$ due to possible error in k_5^r is less than that from the scatter in the measured intensity ratios. The solid curve in fig. 5a represents the best fit to the integrated intensity ratio as a function of added O_2.

Because of the presence of a small amount of O_2 to generate oxygen atoms, the dependence of the integrated intensity ratio on added N_2 density $n(N_2)$ differs somewhat from eq. (12). In this case, we have

$$\frac{I_5}{I_3} = \frac{B}{C+n(N_2)/n_N} + \frac{Dn(N_2)}{C+n(N_2)/n_N}, \tag{15}$$

where

$$B = k_{35}(O_2)\, n(O_2)/k_3^r, \tag{16}$$

$$C = 1+n(O_2)/n_O, \tag{17}$$

$$D = k_{35}(N_2)/k_3^r \tag{18}$$

and

$$n_N = k_5^r/k_5^Q(N_2). \tag{19}$$

The parameters B and C are known from the analysis of the O_2 data. We have not studied the quenching of the ^5P state by N_2. In view of the similarity of the ^3P and ^5P quenching rate constants by O_2, within the large experimental uncertainties particularly of the latter, we assume that $k_5^Q(O_2)$ in eq. (19) equals the corresponding rate constant for the ^3P state. We thus calculate n_N to equal 3.4×10^{16} molecules cm^{-3} cm^{-3} (or 1.05 Torr).

The transfer rate constant $k_{35}(N_2)$ may be calculated by a linear least-squares fit, similar to that used for the corresponding rate constant for O_2, to determine the parameter D in eq. (15). We find that $k_{35}(N_2)$ equals 2×10^{-11} molecule^{-1} cm^3 s^{-1}, with an estimated factor of 2 uncertainty. The solid curve

in fig. 5b represents the best fit to the integrated intensity ratio as a function of added N_2. This value for $k_{35}(N_2)$ depends on assuming that the ^3P and ^5P quenching rate constants for N_2 are the same. If the ^5P rate were only half as large, then the derived value for $k_{35}(N_2)$ would be reduced by $\approx 30\%$, which is within the estimated experimental uncertainties. To show that $^3P \rightarrow {}^5P$ collisional transfer is significant with N_2 collision partner, we have also plotted with a dotted curve in fig. 5b the expected integrated intensity ratio if $k_{35}(N_2)$ were equal to zero. The rate constants k_{35} for both O_2 and N_2 are also included in table 1.

4. Discussion

Table 1 compares our quoted $3p\,^3P$ total quenching rate constants with those determined in previous studies. Our value for O_2 agrees well with that of Bamford et al. [9] and is somewhat higher than the most recent result [7] from Kohse-Höinghaus and co-workers. The present result for the corresponding rate constant for quenching by N_2 is also slightly higher than that of Kohse-Höinghaus and co-workers [7]. By contrast, the earliest measurement of the N_2 quenching rate constant by Bischel et al. [1] is considerably smaller than the present result and that of ref. [7]. We do not know the reason for this discrepancy.

The present result for the $3p\,^3P$ radiative lifetime (33.6 ± 1.7 ns), derived from the intercept of the Stern–Volmer plot for ^3P quenching by O_2 (fig. 4a), agrees reasonably well with previous determinations of this lifetime. By similar observation of time-resolved two-photon laser-induced fluorescence, Bamford et al. [9], Bittner et al. [7], and Kröll et al. [20] obtain values of 34.7 ± 3.7, 36.2 ± 0.69, and 36 ± 4 ns, respectively. The measurement of Bischel et al. [1], who also monitored the emission after two-photon laser excitation and report $\tau(3p\,^3P) = 39.1 \pm 1.4$ ns, and that of Bromander et al. [21], who employed a high frequency electron beam deflection technique and find $\tau(3p\,^3P) = 40 \pm 3$ ns, yield lifetimes somewhat longer than the more recent experimental results. There have been several earlier determinations, involving absolute emission intensity measurements, of the $3p\,^3P \rightarrow 3s\,^3S$ radiative decay rate, and hence $3p\,^3P$ radiative lifetime, since the upper state has only one electric-dipole-allowed decay pathway. The compilation of Wiese et al. [22] gives a value of $\tau(3p\,^3P) = 35.7$ ns. The theoretical calculations of Pradhan and Saraph [23] yields a somewhat smaller result: $\tau(3p\,^3P) = 30.3$ ns. The former is in reasonable agreement with recent time-resolved experiments, while the latter appears to be slightly small.

Our experimental determination of the $3p\,^5P$ radiative lifetime, $\tau(3p\,^5P) = 50 \pm 9$ ns, appears to be somewhat longer than previous estimates of this quantity. The present measurement suffers from difficulties in extracting the ^5P decay rate k_5 in a non-linear least-squares fit to $^5P \rightarrow {}^5S$ emission waveforms with low signal to noise ratio such as that displayed in fig. 3b. There has been only one other time-resolved determination of the $3p\,^5P$ radiative lifetime. Using the high-frequency electron beam deflection technique, Bromander et al. [21] report $\tau(3p\,^5P) = 39 \pm 2$ ns. The compilation of Wiese et al. [22] yields a value of 29 ns, while a result of 28 ns is obtained from the calculations of Pradhan and Saraph [23]. The oscillator strengths computed by Pradhan and Saraph [23] have recently been shown by comparison with electron scattering results to be reliable to better than 20%, at least for transitions out of the ground $2p^4\,^3P$ state [24].

To our knowledge, there have been no previous experimental determinations of collisional properties of the $3p\,^5P$ state. While the exact value for the ^5P quenching rate constant by O_2 may be uncertain because of difficulties such as those discussed in the previous paragraph, the present experiment nevertheless indicates that this quenching is large and comparable to that for the neighboring ^3P state. In attempting to understand the variation of the rate constants for quenching of the nitrogen atom $3p\,^4D$ state by the inert gases, Copeland et al. [8] noted the importance of the availability of excited states in both the excited atom and the quencher to understand the mechanism of quenching. For the oxygen atom, it is interesting that the overall quenching rate for the $3p\,^3P$ and ^5P states by O_2 are both large, despite the fact that the former can be removed by excitation transfer to the ^5P state, which lies only ≈ 2000 cm^{-1} lower, while excitation transfer to lower O atom 3s states for the latter would require removal of ≈ 12000

cm^{-1} (see fig. 1). This suggests that excited states of the O_2 collision partner may be of importance.

The ratio of the rate constants $k_{35}(M)$ to $k_3^Q(M)$ equals the fraction f_T of ^3P quenching collisions which result in excitation transfer to the lower-lying ^5P state. Despite the factor of 2 uncertainty in our measured excitation transfer rate constants, it is nevertheless clear that $^3P \rightarrow {}^5P$ collisional transfer explains only a small fraction of the ^3P quenching. For O_2 and N_2, we find that f_T equals approximately 8% and 3%, respectively. While f_T is significantly lower for the closed-shell N_2 molecule than for O_2, nevertheless this excitation transfer process is not insignificant for the former. This suggests that the model for this process given in section 1 be too simplistic.

We surmise that the bulk of ^3P quenching collisions occurs by excitation transfer to the collision partner, rather than collision-induced transitions to lower-lying oxygen atom states. This intermolecular excitation transfer would be expected to populate quencher electronic states whose energies lie close to that of the incident ^3P state. The initial internal energy of the former is quite high, $\approx 88600\ cm^{-1}$ (see fig. 1), and both O_2 and N_2 possess a number of potential acceptor excited electronic states in this energy range [25]. As the initial excitation energy is greater than the O_2 and N_2 bond energies, dissociative excitation transfer can also occur.

The participation of excited acceptor states in the collisional decay of the ^3P state would explain why the model for $^3P \rightarrow {}^5P$ collision-induced transitions given in section 1 is inadequate. Verification of the importance of intermolecular excitation transfer in the quenching of the $3p\ ^3P$ state could be obtained by observation of excited molecular emission, in the same way that we have shown the existence of intramolecular $^3P \rightarrow {}^5P$ collisional transitions. For example, in the case of N_2 the well-known $C\ ^3\Pi_u$ state has excitation energy very close to that of the O atom ^3P state; this electronic state emits in the second positive system in the ultraviolet [25]. Quenching of the ^3P state by N_2 can also proceed by a chemical path, namely $O(3p\ ^3P) + N_2 \rightarrow NO + N$.

The large uncertainties in the rate constant $k_{35}(M)$ result from the large scatter in the measured integrated intensity ratios I_5/I_3 (see fig. 5). These fluctuations would be considerably reduced if the integrated signals I_5 and I_3 were measured simultaneously with two photomultiplier detectors, rather than sequentially as in the present experiment. In this way, the intensity ratio would be corrected for shot-to-shot fluctuations in the laser pulse energy and spectral profile. Unfortunately, modification of the apparatus to allow dual photomultiplier detection was not possible in this experimental study.

Acknowledgement

We are endebted to Dr. Chen Hsu, of CRDEC at Edgewood, MD, for the loan of a frequency mixing crystal while our crystal was being repolished. BEF and AWM acknowledge partial support from the Air Force Office of Scientific Research, Directorate of Aerospace Sciences, contract number 88-0013. The work at Johns Hopkins University was supported in part by the National Science Foundation and the US Army Research Office.

References

[1] W.K. Bischel, B.E. Perry and D.R. Crosley, Chem. Phys. Letters 82 (1981) 85; Appl. Opt. 21 (1982) 1419.
[2] R.P. Lucht, J.T. Salmon, G.B. King, D.W. Sweeney and N.M. Laurendeau, Opt. Letters 8 (1983) 365.
[3] M. Aldén, H. Edner, P. Grafstrom and S. Svanberg, Opt. Commun. 42 (1982) 244.
[4] M. Aldén, A.L. Schawlow, S. Svanberg, W. Wendt and P.L. Zhang, Opt. Letters 9 (1984) 211.
[5] A.W. Miziolek and M.A. DeWilde, Opt. Letters 9 (1984) 390.
[6] U. Meier, K. Kohse-Höinghaus and Th. Just, Chem. Phys. Letters 126 (1986) 567.
[7] J. Bittner, K. Kohse-Höinghaus, U. Meier and Th. Just, Chem. Phys. Letters, submitted for publication.
[8] R.A. Copeland, J.B. Jeffries, A.P. Hickman and D.R. Crosley, J. Chem. Phys. 86 (1987) 4876.
[9] D.J. Bamford, L.E. Jusinski and W.K. Bischel, Phys. Rev. A 34 (1986) 185.
[10] J.E.M. Goldsmith, Opt. Letters 7 (1982) 437; J. Chem. Phys. 78 (1983) 1610.
[11] J.E.M. Goldsmith, in: Twentieth Symposium (International) on Combustion (The Combustion Institute, Pittsburgh, 1984) p. 1331.
[12] J.E.M. Goldsmith, Appl. Opt. 26 (1987) 566.
[13] P.J.H. Tjossem and T.A. Cool, Chem. Phys. Letters 100 (1983) 479.

[14] M. Aldén, H.M. Hertz, S. Svanberg and S. Wallin, Appl. Opt. 23 (1984) 3255.
[15] J.E.M. Goldsmith and R.J.M. Anderson, Appl. Opt. 24 (1985) 607.
[16] C.E. Moore, Atomic energy levels, Vol. 1, NSRDS-NBS 35 (US Govt. Printing Office, Washington, 1971).
[17] M.H. Alexander, private communication.
[18] M.A.A. Clyne and W.S. Nip, in: Reactive intermediates in the gas phase, ed. D.W. Setser (Academic Press, New York, 1979) p. 1.
[19] P.R. Bevington, Data reduction and error analysis for the physical sciences (McGraw-Hill, New York, 1969).
[20] S. Kröll, H. Lundberg, A. Presson and S. Svanberg, Phys. Rev. Letters 55 (1985) 284.
[21] J. Bromander, N. Duric, P. Erman and M. Larsson, Physica Scripta 17 (1978) 119.
[22] W.L. Wiese, M.W. Smith and B.M. Glennon, Atomic transition probabilities, Vol. 1, NSRDS-NBS 4 (US Govt. Printing Office, Washington, 1966).
[23] A.K. Pradhan and H.E. Saraph, J. Phys. B 10 (1977) 3365.
[24] J.P. Doering, E.E. Gulcicek and S.O. Vaughan, J. Geophys. Res. 90 (1985) 5279.
[25] K.P. Huber and G. Herzberg, Molecular spectra and molecular structure, Vol. 4, Constants of diatomic molecules (Van Nostrand Reinhold, New York, 1979).